

Where Plants Make Oxygen: A Structural Model for the Photosynthetic Oxygen-Evolving Manganese Cluster

Vittal K. Yachandra, Victoria J. DeRose,* Matthew J. Latimer, Ishita Mukerji,† Kenneth Sauer, Melvin P. Klein‡

In the photosynthetic evolution of oxygen, water oxidation occurs at a catalytic site that includes four manganese atoms together with the essential cofactors, the calcium and chlorine ions. A structural model and a determination of the manganese oxidation states based on x-ray absorption spectroscopy are presented. The salient features, in both higher plants and cyanobacteria, are a pair of di- μ -oxo bridged manganese binuclear clusters linked by a mono- μ -oxo bridge, one proximal calcium atom, and one halide. In dark-adapted samples, manganese occurs in oxidation states (III) and (IV). Data from oriented membranes display distinct dichroism, precluding highly symmetrical structures for the manganese complex.

The oxidation of water to O_2 is a characteristic reaction associated with photosynthesis in higher plants and cyanobacteria. The oxygen-evolving complex (OEC) of the photosynthetic apparatus that catalyzes this oxidation contains a cluster of four Mn atoms that acts as the locus of charge accumulation. The OEC cycles through a series of five intermediate states (S_i , $i = 0$ to 4) driven by the energy of four successive photons absorbed by the pigment P_{680} of photosystem II (PS II) (1). The ions Ca^{2+} and Cl^- are essential cofactors that can be replaced by Sr^{2+} and Br^- , respectively. The structure of the Mn complex, the mechanism of charge storage, and the eventual oxidation of water to O_2 have been the subject of much study (2–5). The discovery of electron paramagnetic resonance (EPR) signals associated with Mn in particular S states, especially the multiline signal associated with the S_2 state (6), and the application of x-ray absorption spectroscopy (XAS) to the study of Mn in the OEC (7) have had an important influence on this endeavor. A structural model for the Mn complex based on our XAS studies is presented in this report.

The Fourier transform of the Mn extended x-ray absorption fine structure (EXAFS) data of PS II samples from the cyanobacterium *Synechococcus* sp. in the S_1 state shows three well-resolved major peaks (Fig. 1A) (8, 9). In this radial distribution

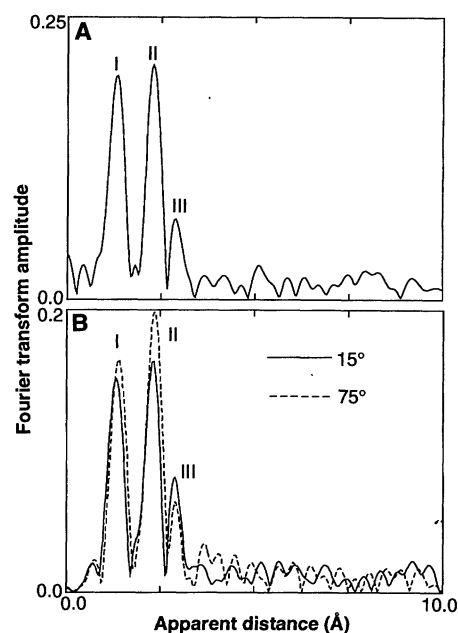
about Mn, each of the Fourier peaks represents x-ray photoelectron backscattering from the coordinating or neighboring atoms, and the EXAFS oscillations represented by the Fourier peaks are described by Eq. 1 (9). The least-squares residual between the Fourier-isolated EXAFS waves and the simulation of these waves with use of the EXAFS equation defines the goodness-of-fit parameter, which provides the criterion for best fits and for the assignment of the Fourier peaks (9).

1) The first Fourier peak (labeled I in Fig. 1A) is best simulated by two shells of O or N ligand atoms. The first shell is modeled as ~ 2 O or N ligand atoms per Mn at ~ 1.82 Å (9). The Mn-O bridging distances are typically about 1.8 to 1.9 Å in multinuclear

μ_2 - or μ_3 -oxo bridged Mn complexes (10), and we therefore assign this shell to O atoms bridging between Mn atoms. The second shell consists of two to four O or N ligand atoms per Mn at distances between 1.95 and 2.15 Å. This range of distances reflects a distribution of bond lengths in the Mn complex similar to those of Mn-O and Mn-N terminal ligands in multinuclear Mn complexes (10). There has been some disagreement about whether the best fit to the first peak consists of one or two shells, but a consensus is emerging that supports our assignment to two shells (11).

2) The second Fourier peak (labeled II in Fig. 1A) is best simulated by a single shell of Mn. The best-fit parameters are consistent with each Mn atom in the OEC having ~ 1.25 Mn neighbors at a distance of 2.72 Å (9). Fitting analysis on the EXAFS alone cannot distinguish between Fe and Mn; however, Fe has not been implicated in the OEC (2), and several EPR studies have demonstrated that the spectra are best simulated by a tetranuclear exchange-coupled Mn cluster (2, 6). Examination of a series of multinuclear Mn(III) and Mn(IV) complexes reveals that the Mn-Mn distances range between 2.6 and 2.8 Å in complexes in which two Mn atoms are bridged by at least two μ_2 -oxo (12, 13) or two μ_3 -oxo bridges (14, 15). An additional μ_2 -carboxylato bridge does not change the Mn-Mn distance significantly (12). The distance decreases to 2.3 Å when the two Mn atoms are linked by three μ_2 -oxo bridges (13) and to 2.53 Å when linked by two μ_2 -oxo and a μ_2 -peroxo bridge (16). The important point is that there exist

Fig. 1. (A) Fourier transforms of the k^3 -weighted Mn EXAFS data (3.5 to 12.0 Å $^{-1}$) from *Synechococcus* in the S_1 state. Peak I represents backscattering from bridging and terminal ligand N or O at ~ 1.8 and 1.95 to 2.15 Å. The goodness-of-fit parameter improves by a factor of 2 to 10 for a two-shell fit compared to a one-shell fit (8, 21). Peak II is attributable to Mn at 2.72 Å (9). Peak III fits to Mn or Ca or both at ~ 3.3 Å. Fourier transforms of EXAFS spectra from samples in the S_1 and S_2 states from spinach and from the S_2 state from *Synechococcus* are similar (8). The apparent distance is shorter than the actual distance to a given neighboring atom because of the effect of the averaged phase of the EXAFS wave. **(B)** Fourier transforms of the k^3 -weighted Mn EXAFS data (3.5 to 11.5 Å $^{-1}$) of oriented PS II membranes in the S_1 state from spinach. The membrane normal was oriented 15° and 75° to the polarization direction of the x-rays. The changes seen in peaks I, II, and III are reproducible, but the other peaks are within the noise level and could not be reproduced. The number of scatterers at 2.7 and 3.3 Å from four different orientations (data from 45° and 55° not shown) has been fit by the method described in (20). The polar plots show that the 2.7 Å Mn-Mn vector is oriented at $60^\circ \pm 10^\circ$ to the membrane normal and the 3.3 Å vector is aligned at $30^\circ \pm 10^\circ$ to the membrane normal.



V. K. Yachandra and M. P. Klein, Structural Biology Division, Lawrence Berkeley Laboratory, University of California, Berkeley, CA 94720.

V. J. DeRose, M. J. Latimer, I. Mukerji, K. Sauer, Structural Biology Division, Lawrence Berkeley Laboratory, and Department of Chemistry, University of California, Berkeley, CA 94720.

*Present address: Department of Chemistry, Northwestern University, Evanston, IL 60208.

†Present address: Department of Chemistry, Princeton University, Princeton, NJ 08544.

‡To whom correspondence should be addressed.

two μ_2 -oxo bridges between pairs of Mn atoms in all reported complexes that have a Mn-Mn distance of about 2.7 Å (10).

3) The third peak in the Fourier transform (labeled III in Fig. 1A) is well fit by a combination of 0.5 Mn and 0.25 Ca interaction per Mn atom at ~ 3.3 Å (9). The peak can also be fit to a combination of Mn and C contributions, but the fit quality is better for the Mn and Ca atoms (also see Fig. 3 caption). Penner-Hahn and co-workers (11) were the first to suggest that the 3.3 Å shell could also be fit with Ca. In complexes that contain two μ_2 -carboxylato bridges and one μ_2 -oxo bridge, the Mn-Mn distance is greater than 3 Å and, in some complexes, is as large as 3.5 Å (14, 17, 18). In complexes where the Mn atoms are linked by a single μ_2 -oxo bridge, as in the adamantane-like complex, the Mn-Mn distance is 3.2 Å (18). Again, the important point is that a Mn-Mn distance of 3.3 Å is characteristic of mono μ_2 -oxo and μ_2 -carboxylato bridges between the Mn atoms (10).

The Fourier transforms of Mn EXAFS data from oriented spinach PS II membranes in the S_1 state (19) are shown in Fig. 1B. The membrane normal was oriented 15° and 75° relative to the polarization direction of the x-ray photons. Fourier peak II, which is characteristic of backscattering from Mn at 2.7 Å, exhibits clear dichroism with a larger amplitude at 75° than at 15°, which suggests that the 2.7 Å vectors are aligned approximately in the plane of the membrane. Fourier peak I, which is dominated by the Mn-O 1.8 Å vector, also shows dichroism similar to that of peak II. This is expected for a model of μ_2 -oxo bridged units lying in the plane of the membrane. The Fourier peak labeled III is also dichroic, but the orientation dependence is opposite to that exhibited by peaks I and II (20), indicating that the resultant 3.3 Å vector lies approximately along the membrane normal.

Questions concerning the oxidation state or states and symmetry of the Mn as functions of S state have been addressed by examination of the x-ray absorption near-edge structure (XANES) region at the Mn K-edge. Previous studies have shown that Mn is oxidized when it advances from the S_0 to the S_1 state (21) and from the S_1 to the S_2 state (8, 22), as evidenced by a shift of the K-edge inflection point to higher energy. By comparison of the inflection-point energy of the Mn K-edge in the OEC with that of various Mn complexes, the oxidation state of Mn in the S_1 state was assigned to $(\text{III})_4$ or $(\text{III})_2(\text{IV})_2$ (7, 8, 22). In addition to the position of the K-edge inflection-point energy, the shape of the K-edge can be informative. The shape of the edge is characterized not only by the oxidation state of the metal but also by the

types of ligand atoms and bond distances to the nearest neighbors (11, 23–25) (Fig. 2A). The second derivatives of the K-edge spectra emphasize the structure and the changes in the features of the spectra (Fig. 2B). We have found, in a study that included over 20 model compounds of varying ligand environment and nuclearity, that in general, the ligand-induced changes in edge shape below 6560 eV are secondary to the changes produced by oxidation state (24).

Simulations of the second derivatives of the XANES of the Mn in PS II by sums of those of model compounds (Fig. 2C) show that there is no Mn(II) in the S_1 state in the OEC, a result that is consistent with the Mn K-edge inflection-point studies (8, 22). Also, the fit to Mn in the S_1 state when the oxidation states $(\text{III})_2(\text{IV})_2$ are used is clearly better than that obtained with the oxidation states $(\text{III})_4$. Small differences are still evident between the simulation con-

taining the oxidation states $(\text{III})_2(\text{IV})_2$ and the S_1 state, perhaps because the Mn complex in the OEC contains more O ligands and fewer N ligands than the Mn complexes used for the simulations. The use of multinuclear model complexes containing oxo and carboxylato bridges does not change the conclusions regarding the oxidation states of Mn in PS II samples (24).

The Ca^{2+} cofactor, which is essential for O_2 evolution, can be replaced by Sr^{2+} (26). Replacement of Ca by Sr decreases the steady-state rate of O_2 evolution, but yields of flash-induced O_2 evolution have shown that all of the centers are active in Sr-reconstituted samples (27). The S_2 -state multiline EPR signal changes markedly when Ca^{2+} is replaced by Sr^{2+} , indicating a structural perturbation of the Mn complex (27). It has been postulated that Ca^{2+} or Sr^{2+} is in the immediate vicinity of the Mn complex and is possibly even bridged to one

Fig. 2. (A) The K-edge spectra of Mn(II), Mn(III), and Mn(IV) complexes. (B) Corresponding second derivatives. There is a dramatic change in shape as well as in inflection-point energy as the oxidation state increases. The complexes are Mn(II)(acac)₂(H₂O)₂, Mn(III)(acac)₃, and Mn(IV)(sal)₂(bipy) (acac, acetylacetonate; bipy, bipyridine; and sal, salicylate). By comparing the edge shape of model compounds with differing nuclearities and bridging environments (24), including a series of oxo- or carboxylato-bridged bi, tri, and tetranuclear complexes, we found that the nature of the immediate ligand affects the region above ~ 6560 eV (where multiple scattering and EXAFS effects become manifest) but that the overall shape, especially below this region, correlates well with oxidation state. We used combinations of simple mononuclear complexes to compare with the PS II Mn K-edge data in (C). Second derivatives were generated by analytical differentiation of a third-order polynomial fit to the data over an interval of ± 2.75 eV on each side of a data point. (C) The second derivative of the Mn K-edge of PS II particles in the S_1 state is shown as a solid line. Dashed lines are the second derivatives of the Mn K-edge spectra created by weighted sums of spectra of the model complexes in different oxidation states (II), (III), or (IV) shown in (A) and (B). The sets of oxidation states for the simulations were chosen to produce a conventional EPR-silent ground state; a prerequisite from studies which show that the OEC in the S_1 state is EPR silent (7, 38). The particular combinations of oxidation states used in the simulations are, for curve 1, $(\text{II})_2(\text{III})_2$; for curve 2, $(\text{II})(\text{III})_2(\text{IV})_2$; for curve 3, $(\text{III})_4$; and for curve 4, $(\text{III})_2(\text{IV})_2$. The combination $(\text{III})_2(\text{IV})_2$ is the most similar to PS II in the S_1 state.

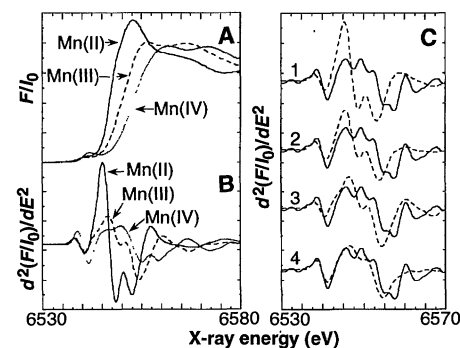
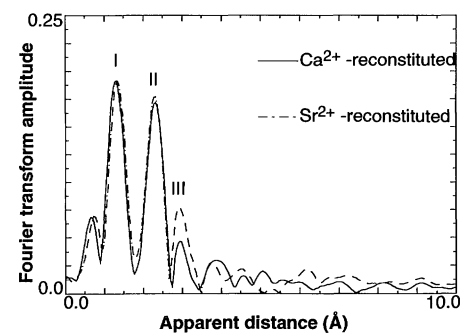


Fig. 3. Fourier transforms of the k^3 -weighted Mn EXAFS data (3.5 to 12.0 Å⁻¹) of Ca^{2+} -depleted samples reconstituted with Ca^{2+} (solid line) or with Sr^{2+} (dashed line). Peaks I and II are similar between the two preparations and closely resemble the Fourier transforms of the EXAFS from untreated samples (Fig. 1A). Peak III, however, exhibits a markedly increased amplitude for the Sr^{2+} -reconstituted preparation. Depletion of Ca^{2+} was carried out by the method of Ono and Inoue (28). It is generally more difficult to obtain unique fits for peaks at distances greater than 3 Å, so contour plots were constructed of the goodness-of-fit parameter as a function of the number of Mn-C, Mn-Mn, and Mn-Ca (or Mn-Sr) scatterers. In each case, the contours showed a minimum at one Mn-Mn and one Mn-Ca or Sr contribution to the third peak. The minima in the contours were better defined for the Sr plots than for the Ca plots, which is to be expected because Sr is a better backscatterer and produces a greater contribution to the EXAFS spectrum.



Mn (28). The Mn EXAFS studies in which Ca^{2+} -depleted S_1 -state samples are reconstituted with Sr^{2+} show an increase in the amplitude of peak III in the Fourier transform (Fig. 3), thus providing evidence for the close proximity of this element to Mn. The increase in amplitude is consistent with replacement of Ca^{2+} by Sr^{2+} , which is a more effective backscatterer. Simulations of the EXAFS spectra from both the Sr^{2+} -reconstituted sample and the Ca^{2+} -reconstituted sample show that the first two peaks in the Fourier transform are similar to those in the native S_1 sample. The major difference is in the fitting parameters to the third peak from the Sr^{2+} -reconstituted sample; it shows an increased amplitude and is best fit by 0.5 Mn and 0.25 Sr (instead of

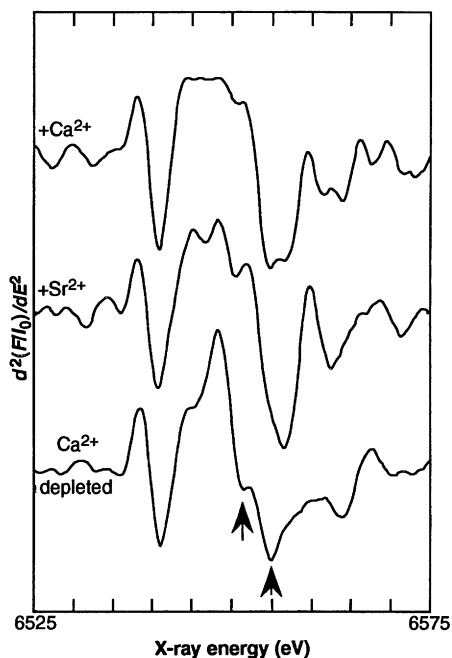


Fig. 4. The second derivatives of the Mn K-edge spectra of a Ca^{2+} -depleted sample and samples reconstituted with Ca^{2+} or Sr^{2+} in the S_1 state. Arrows point to areas where the greatest changes in shape occur in the spectra of the Ca^{2+} -depleted sample. Second derivatives were generated according to the procedure described in Fig. 2 caption.

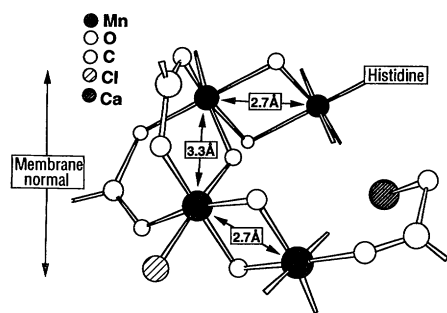


Fig. 5. Proposed model for the Mn complex in photosystem II (34).

Ca) backscatterer at $\sim 3.3 \text{ \AA}$ (9) (Fig. 3).

Depletion of Ca^{2+} by NaCl wash (26) or by a low-pH treatment (28) results in an S_2 -state multiline EPR signal that is stable in the dark, which differs from the signal obtained from preparations containing either Ca^{2+} or Sr^{2+} (29–31). The Ca^{2+} -depleted samples do not advance beyond the S_3 state, and this S_3 state is characterized by a $g = 2$ EPR signal, which has been assigned to a histidine radical interacting with the Mn cluster (29–31). Inhibition of O_2 evolution and the modification of the multiline EPR signal upon Ca^{2+} depletion suggest that the Mn cluster is perturbed. Small changes in the shape of the Mn K-edges in the Ca^{2+} - and Sr^{2+} -reconstituted samples can be seen in Fig. 4, as well as the dramatic changes in shape in the Ca^{2+} -depleted S_1 state. Similar changes have been reported by Ono and Inoue (28). Such a large change in edge shape is a clear indication that removal of Ca^{2+} perturbs the structure of the Mn complex.

The Cl^- cofactor is also essential for O_2 evolution and can be replaced by Br^- with retention of activity, but F^- is an inhibitor of O_2 evolution (5). The activity of Br^- -reconstituted samples is reported to be 80 to 100% of that in samples containing Cl^- (5, 32). In our trials, the activity of Br^- -reconstituted samples is 95% or higher compared with that of control samples (8). The requirement of Cl^- or Br^- for activity has led to the postulate that a halide ion is a ligand to one or more of the Mn atoms in the cluster (32, 33). We have grown the thermophilic cyanobacterium *Synechococcus* sp. on medium containing only Br^- , a more efficient backscatterer in the XAS experiment. Only subtle differences in the Mn EXAFS data between Cl^- - and Br^- -grown organisms were found. Fits to the data preclude the existence of two halide ligands or a halide bridging ligand but cannot exclude one halide backscatterer per four Mn atoms (8).

In this same context, we have examined the XAS features of a spinach preparation inhibited with 25 mM F^- . Fluoride binds at the same site as does the tightly bound Cl^- and Br^- (32). The second peak in the Fourier transform of these data is best simulated by the inclusion of two Mn-Mn distances, one at 2.68 and another at 2.84 Å . The fit quality improves, and the goodness-of-fit parameter improves by a factor of 2.5 on the inclusion of the second distance. When forced to fit to a single distance, the Debye-Waller parameter is larger than that obtained for the control samples. These results suggest that F^- binds to one of the di- μ -oxo bridged binuclear centers, thereby perturbing one of the Mn-Mn distances, and provide evidence supporting our assignment of pairs of di- μ -oxo bridged binuclear

Mn moieties as the central constituents of the cluster.

On the basis of the foregoing observations and interpretations, we propose a model for the Mn cluster (Fig. 5) (34):

1) EXAFS analysis supports at least one Mn-Mn vector at a distance of 2.7 Å and 0.5 Mn-Mn vector at 3.3 Å per Mn atom in the cluster. We propose that there are minimally two di- μ -oxo bridged binuclear structures with a Mn-Mn separation of 2.7 Å , which in turn are linked with a 3.3 Å separation by mono- μ -oxo and mono- or di-carboxylato bridges. The dichroism studies are consistent with an alignment of the 2.7 Å vectors approximately parallel to the plane of the membrane. The arrangement of Mn atoms that we propose is based on a straightforward interpretation of the available data, but we cannot rule out, for example, a structure in which the two 2.7 Å Mn-Mn vectors are aligned trans to the 3.3 Å Mn-Mn vector (in the structure shown, they are aligned cis with respect to the 3.3 Å Mn-Mn vector) or a structure that consists of a 2.7 Å bridge between a 2.7 and 3.3 Å vector, whereas the structure in Fig. 5 shows a 3.3 Å bridge between two 2.7 Å vectors. The presence of about one Mn backscatterer per Mn atom at 2.7 Å provides conclusive evidence against the symmetric cubane clusters proposed by Brudvig and Crabtree (35) and the "butterfly" tetranuclear clusters proposed by Christou and Vincent (36) as possible candidates for the Mn complex in the OEC. The number of Mn backscatterers at 2.7 Å are 3 and 0.5 (average per Mn) for the symmetric cubane and the butterfly structure, respectively. A symmetric cubane-like structure is also inconsistent with the dichroism of the XAS data; however, we cannot rule out a highly distorted cubane-like or trigonal pyramidal structure (15).

2) The Mn K-edge results are best simulated with oxidation states of $(\text{III})_2(\text{IV})_2$ in the S_1 state and $(\text{III})(\text{IV})_3$ in the S_2 state (24). The assignment of $(\text{III})_2(\text{IV})_2$ to the S_1 state is consistent with an EPR-silent ground state. We propose that in the S_1 state, one of the di- μ -oxo centers is in the $(\text{III})_2$, the other is in the $(\text{IV})_2$ oxidation state, and each of the binuclear centers is antiferromagnetically coupled, as are all known di- μ -oxo bridged models (10). The two centers are also coupled to each other antiferromagnetically, leading to an $S = 0$, EPR-silent ground state (37, 38).

3) Perturbation of the Mn K-edge upon Ca^{2+} depletion and the increase in amplitude of the third Fourier peak on replacement of Ca^{2+} with Sr^{2+} provide evidence that Ca^{2+} is located near Mn; in Fig. 5, we show them bridged by a carboxyl group. Other possible bridging ligands are oxo or phenoxy (tyrosine-derived) groups or histidine.

4) XAS data show that F^- perturbs one of the di- μ -oxo bridged Mn-Mn distances, presumably by binding to one of the di- μ -oxo centers. Fluoride is known to be a competitive inhibitor of Cl^- (32). As described above, there is EXAFS evidence against a halide bridging between two Mn. On the basis of these results, we show Cl^- as a terminal ligand to Mn in Fig. 5 (8). Furthermore, EPR studies show (8, 39) that replacement of Cl^- by F^- changes the S_2 -state EPR signal from a $g = 2$, $S = 1/2$ ground state to a $g = 4.1$, $S = 5/2$ ground state. We postulate that Cl^- or F^- modulates the magnetic coupling between the two di- μ -oxo moieties so that it is antiferromagnetic in the case of Cl^- and ferromagnetic in the case of F^- ; in the first case, it leads to a $S = 1/2$ ground state and the multiline EPR signal, and in the second case, to a $S = 5/2$ ground state and the $g = 4.1$ EPR signal (37, 40). We therefore place the halide ligand in a position trans to the mono- μ -oxo bridge, linking the two di- μ -oxo bridged binuclear clusters, a position well suited for the modulation of the coupling between the two di- μ -oxo bridged moieties (37).

5) Finally, we append a histidine to one of the Mn as a terminal ligand (Fig. 5). This assignment is based on our observation of the difference in the electron spin echo envelope modulation (ESEEM) of the S_2 -state multiline EPR signal of *Synechococcus* grown in ^{14}N and ^{15}N . A feature at about 5-MHz ESEEM in samples from the lighter isotope is absent from the ^{15}N -grown samples (41).

REFERENCES AND NOTES

- B. Kok, B. Forbush, M. McGloin, *Photochem. Photobiol.* **11**, 457 (1970).
- A. W. Rutherford, J.-L. Zimmermann, A. Boussac, in *The Photosystems: Structure, Function, and Molecular Biology*, J. Barber, Ed. (Elsevier, Amsterdam, 1992), pp. 179–229; G. T. Babcock, in *New Comprehensive Biochemistry in Photosynthesis*, J. Amesz, Ed. (Elsevier, Amsterdam, 1987), vol. 15, pp. 125–158; G. W. Brudvig, in *Advanced EPR Applications in Biology and Biochemistry*, A. J. Hoff, Ed. (Elsevier, Amsterdam, 1990), pp. 839–863.
- R. J. Debus, *Biochim. Biophys. Acta* **1102**, 269 (1992).
- Role of Ca reviewed by C. F. Yocum, in *Manganese Redox Enzymes*, V. L. Pecoraro, Ed. (VCH Publishers, New York, 1992), pp. 71–83; *Biochim. Biophys. Acta* **1059**, 1 (1991).
- Role of halide reviewed by W. J. Coleman, *Photosynth. Res.* **23**, 1 (1990); P. H. Homann, *J. Bioenerg. Biomembr.* **19**, 105 (1987).
- G. C. Dismukes and Y. Siderer, *Proc. Natl. Acad. Sci. U.S.A.* **78**, 274 (1981); Ö. Hansson and L.-E. Andréasson, *Biochim. Biophys. Acta* **679**, 261 (1982); J. Bonvoisin, G. Blondin, J.-J. Girerd, J.-L. Zimmermann, *Biophys. J.* **61**, 1076 (1992); M. Kusunoki, in *Research in Photosynthesis*, N. Murata, Ed. (Kluwer, Dordrecht, Netherlands, 1992), vol. II, pp. 279–300; M. Zheng and G. C. Dismukes, in *ibid.*, pp. 305–308.
- Reviewed by K. Sauer, V. K. Yachandra, R. D. Britt, M. P. Klein, in *Manganese Redox Enzymes*, V. L. Pecoraro, Ed. (VCH Publishers, New York, 1992), pp. 141–175.
- V. J. DeRose, thesis, University of California, Berkeley (1990); *Lawrence Berkeley Laboratory Report LBL-29795* (Univ. of California, Berkeley, 1990); A. E. McDermott *et al.*, *Biochemistry* **27**, 4021 (1988).
- All XAS spectra were collected at 10 K with a solid-state Ge detector in the fluorescence mode. The EXAFS oscillations $\chi(k)$ are described as a function of the magnitude of the photoelectron wave vector, k , for a given absorbing atom (Mn) with N_j backscattering neighbors j at a distance r_j by the following equation

$$\chi(k) = \sum_j \frac{N_j}{k r_j^2} f_j(k, \pi) e^{-2\sigma_j^2 k^2} \sin[2kr_j + \Psi_j(k)] \quad (1)$$
 where the backscattering amplitude f_j is a function of the atomic number of the backscattering element, $k = [(2m_e/h^2)(E - E_0)]^{1/2}$, m_e is the electron mass, h is Planck's constant, and E_0 is the threshold energy for photoionization. The function Ψ_j includes the phase shift from the central-atom absorber as well as the backscattering element. The Debye-Waller factor σ describes the attenuating effect caused by static and thermal disorder. The Mn EXAFS data from PS II samples were fit with theoretical values for the backscattering amplitude and phase shifts for the scattering and absorbing atoms, which were calculated with the curved-wave formalism of A. G. McKale, B. W. Veal, A. P. Paulikas, S.-K. Chan, and G. S. Knapp [*J. Am. Chem. Soc.* **110**, 3763 (1988)]. The fitting procedures are described in detail in (8, 21). The estimated fit parameters for the first Fourier peak are 2 ± 0.2 for the coordination number and $1.82 \pm 0.01 \text{ \AA}$ for the O distance; for the second Fourier peak, 1.25 ± 0.25 Mn backscatters and $2.72 \pm 0.01 \text{ \AA}$ distance; for the third Fourier peak, 0.5 ± 0.1 Mn backscatterer at $3.3 \pm 0.1 \text{ \AA}$ and 0.25 ± 0.1 Ca (or Sr for Sr^{2+} -reconstituted samples) backscatterer at $3.3 \pm 0.1 \text{ \AA}$. The Debye-Waller parameters were 0.002 to 0.005 \AA^2 for the first and second peaks and 0.005 to 0.01 \AA^2 for the third peak. These numbers compare well with Debye-Waller parameters derived from multinuclear Mn complexes. The parameter ΔE_0 in the simulations allowed variance of ± 20 eV from E_0 , which was the energy at maximum peak height of the Mn K-edge.
- K. Wieghardt, *Angew. Chem. Int. Ed. Engl.* **28**, 1153 (1989); V. L. Pecoraro, in *Manganese Redox Enzymes*, V. L. Pecoraro, Ed. (VCH Publishers, New York, 1992), pp. 197–231.
- J. E. Penner-Hahn *et al.*, *J. Am. Chem. Soc.* **112**, 2549 (1990). The results obtained by Penner-Hahn *et al.* with purified OEC preparations from spinach that lack the 17- and 24-kDa polypeptides are very similar to those described here except for the assignment of the Mn-O bridging distances. The discrepancy between our simulations and those of Penner-Hahn *et al.* and George, Prince, and Cramer (20), which required only one longer distance to fit peak I, is most likely attributable to the presence of Mn^{2+} contamination in their samples. Both groups have acknowledged the presence of Mn(II) contamination (3, 42). This will increase the deduced average bond length for Mn [S. Cramer, personal communication in (3)], which, for both studies, obviated the requirement of a shorter shell at about 1.8 \AA for attainment of a statistical best fit to their data. It should also be noted that Penner-Hahn *et al.* did not exclude the possibility of a shorter 1.75 to 1.8 \AA interaction. More recent data collected by Cramer, which shows no Mn^{2+} contamination, does require a short Mn-O shell at $\sim 1.8 \text{ \AA}$ [S. Cramer, personal communication in (8)]. Two other reports have also shown that two shells are required to fit the first Fourier peak [D. J. MacLachlan *et al.*, *Biochem. J.* **285**, 569 (1992); A. R. Corrie, M. C. W. Evans, J. A. M. Hubbard, R. W. Strange, S. S. Hasnain, in *Current Research in Photosynthesis*, M. Baltscheffsky, Ed. (Kluwer, Dordrecht, Netherlands, 1990), vol. 1, pp. 793–796].
- P. M. Plaksin, R. C. Stoufer, M. Mathew, G. J. Palenik, *J. Am. Chem. Soc.* **94**, 2121 (1972); M. Stebler, A. Ludi, H.-B. Bürgi, *Inorg. Chem.* **25**, 4743 (1986); K. Wieghardt *et al.*, *J. Chem. Soc. Chem. Commun.* **1987**, 651 (1987).
- K. Wieghardt *et al.*, *J. Am. Chem. Soc.* **110**, 7398 (1988).
- J.-B. Vincent *et al.*, *J. Chem. Soc. Chem. Commun.* **1987**, 236 (1987); C. Christmas *et al.*, *ibid.*, p. 1303.
- J. S. Bashkin *et al.*, *J. Am. Chem. Soc.* **109**, 6502 (1987).
- U. Bossek, T. Weyhermüller, K. Wieghardt, B. Nuber, J. Weiss, *ibid.* **112**, 6387 (1990).
- K. Wieghardt, U. Bossek, D. Ventur, J. Weiss, *J. Chem. Soc. Chem. Commun.* **1985**, 347 (1985); J. E. Sheats *et al.*, *J. Am. Chem. Soc.* **109**, 1435 (1987); K. Wieghardt *et al.*, *Angew. Chem.* **98**, 1026 (1986).
- K. Wieghardt, U. Bossek, W. Gebert, *Angew. Chem.* **95**, 320 (1983).
- We prepared the oriented samples by layering PS II membranes on a metal-free Mylar tape and slowly drying them in a stream of cold N_2 gas. We determined orientation by monitoring the EPR signal from *cyt b₅₅₉*, which exhibits distinct g anisotropy, and the EPR spectrum of D^+ (tyrosine radical), which shows characteristic orientation dependence [A. W. Rutherford, *Biochim. Biophys. Acta* **805**, 189 (1985)]. The mosaic spread of the oriented membranes has been determined by EPR spectroscopy [H. Blum, J. C. Salerno, J. S. Leigh, *J. Magn. Reson.* **30**, 385 (1978)] to be between 20° and 25° , depending on the sample.
- Our K-edge dichroism spectra (24) and Fourier transforms of EXAFS data (Fig. 1B) are dramatically different from those reported by G. N. George, R. C. Prince, S. P. Cramer [*Science* **243**, 789 (1989)]. We have been able to simulate their spectra by adding about 40% Mn(II) to our spectra (7). The contaminating Mn(II) [Mn(II)-O distances are typically 2.2 \AA] leads to overestimates of the Mn-O or N distances (17) and distorts the amplitude of the Fourier peaks. It explains the major differences seen in the intensities of the Fourier peaks reported by George *et al.* and those shown in Fig. 1B. The second peak in our data is best fit to 1.25 ± 0.25 Mn-Mn vectors at 2.72 \AA , which is significantly different from the 2.1 ± 0.8 Mn-Mn interactions at 2.7 \AA reported by George *et al.*
- R. D. Guiles *et al.*, *Biochemistry* **29**, 486 (1990).
- D. B. Goodin, V. K. Yachandra, R. D. Britt, K. Sauer, M. P. Klein, *Biochim. Biophys. Acta* **767**, 209 (1984); V. K. Yachandra *et al.*, *Biochemistry* **26**, 5974 (1987); J. Cole *et al.*, *Biochim. Biophys. Acta* **890**, 395 (1987); M. Kusunoki, T. Ono, T. Matsushita, H. Oyanagi, Y. Inoue, *J. Biochem. Tokyo* **108**, 560 (1990); T.-A. Ono *et al.*, *Science* **258**, 1335 (1992).
- C. R. Natoli, *Springer Ser. Chem. Phys.* **27**, 43 (1983); A. Bianconi *et al.*, *Biochem. Biophys. Res. Commun.* **131**, 98 (1985).
- V. K. Yachandra *et al.*, unpublished data.
- S. D. Conradson *et al.*, *J. Am. Chem. Soc.* **107**, 7935 (1985).
- D. F. Ghanotakis, G. T. Babcock, C. F. Yocum, *FEBS Lett.* **167**, 127 (1984).
- A. Boussac and A. W. Rutherford, *Biochemistry* **27**, 3476 (1988).
- T.-A. Ono and Y. Inoue, *FEBS Lett.* **227**, 147 (1988).
- A. Boussac, J.-L. Zimmermann, A. W. Rutherford, *Biochemistry* **28**, 8984 (1989).
- M. Sivaraja, J. Tso, G. C. Dismukes, *ibid.*, p. 9459.
- T.-A. Ono and Y. Inoue, in *Current Research in Photosynthesis*, M. Baltscheffsky, Ed. (Kluwer, Dordrecht, Netherlands, 1990), vol. I, pp. 741–744; T.-A. Ono, M. Kusunoki, T. Matsushita, H. Oyanagi, Y. Inoue, *Biochemistry* **30**, 6836 (1991).
- P. O. Sandusky and C. F. Yocum, *FEBS Lett.* **162**, 339 (1983); *Biochim. Biophys. Acta* **849**, 85 (1986).
- A. W. Rutherford, *Trends Biochem. Sci.* **14**, 227 (1989).
- Although we have provided evidence for the tetranuclear Mn model and the presence of Ca, halide, and histidine, as shown in Fig. 5, we do not know their positions relative to each other at this time.

35. G. W. Brudvig and R. H. Crabtree, *Proc. Natl. Acad. Sci. U.S.A.* **83**, 4586 (1986).
36. G. Christou and J. B. Vincent, *Biochim. Biophys. Acta* **895**, 259 (1987).
37. O. Burghaus, V. J. DeRose, W. Liang, V. K. Yachandra, M. P. Klein, in *Research in Photosynthesis*, N. Murata, Ed. (Kluwer, Dordrecht, Netherlands, 1992), vol. II, pp. 109–113.
38. Here, EPR silent refers to a conventional EPR experiment in which one detects transitions in a half-integral spin system. However, we have detected paramagnetism in the S_1 state by using parallel-polarization-mode EPR, a method used for observing EPR transitions from integer or non-Kramers spin systems. S. L. Dexheimer and M. P. Klein, *J. Am. Chem. Soc.* **114**, 2821 (1992).
39. A. Haddy, W. R. Dunham, R. H. Sands, R. Aasa, *Biochim. Biophys. Acta* **1099**, 25 (1992).
40. We propose that the coupling within the $Mn_2(III,IV)$ and $Mn_2(IV,IV)$ units is antiferromagnetic. Ferromagnetic coupling of the $S = 1/2$ ground state of the $Mn_2(III,IV)$ cluster with a $S = 2$ excited state of the $Mn_2(IV,IV)$ cluster results in the formation of the $\tilde{S} = 5/2$ ground state. Antiferromagnetic coupling of the $S = 1/2$ ground state of the $Mn_2(III,IV)$ cluster with the $S = 0$ state of the $Mn_2(IV,IV)$ cluster results in an $S = 1/2$ state.
41. V. J. DeRose *et al.*, *Biochemistry* **30**, 1335 (1991).
42. J. J. Riggs, R. Mei, C. F. Yocum, J. E. Penner-Hahn, *J. Am. Chem. Soc.* **114**, 10650 (1992).
43. We thank W. Armstrong, G. Christou, T. Collins, J.-J. Girerd, D. Hodgson, and K. Wieghardt for providing all of the Mn model complexes. We thank H. Dau, T. Roelofs, W. Liang, and J. Andrews for discussions about this work. We are grateful to D. B. Goodin, A. E. McDermott, R. D. Guiles, J. L. Cole, R. D. Britt, J.-L. Zimmermann, S. L. Dexheimer, and D. Kim for their contributions, and to M. Grush for help with XAS data collection. This work was supported by National Science Foundation grant DMB91-04104 and by the director, Division of Energy Biosciences, Office of Basic Energy Sciences, Department of Energy (DOE), under contract DE-AC03-76SF00098. M.P.K. thanks the A. von Humboldt Foundation for a Senior U.S. Scientist Award. Synchrotron radiation facilities were provided by the Stanford Synchrotron Radiation Laboratory (SSRL) and the National Synchrotron Light Source (NSLS), both supported by DOE. The Biotechnology Laboratory at SSRL and Beam Line X9-A at NSLS are supported by the National Center for Research Resources of the National Institutes of Health.

23 November 1992; accepted 1 March 1993

Reversal of Left-Right Asymmetry: A Situs Inversus Mutation

Takahiko Yokoyama, Neal G. Copeland, Nancy A. Jenkins, Charles A. Montgomery, Frederick F. B. Elder, Paul A. Overbeek*

A recessive mutation was identified in a family of transgenic mice that resulted in a reversal of left-right polarity (situs inversus) in 100 percent of the homozygous transgenic mice tested. Sequences that flanked the transgenic integration site were cloned and mapped to mouse chromosome 4, between the *Tsha* and *Hxb* loci. During early embryonic development, the direction of postimplantation turning, one of the earliest manifestations of left-right asymmetry, was reversed in homozygous transgenic embryos. This insertional mutation identifies a gene that controls embryonic turning and visceral left-right polarity.

The establishment of embryonic axes is essential for vertebrate development, but the molecular factors that define vertebrate embryonic polarity remain unknown. Left-right asymmetries are the last to appear in embryonic development and are reflected in the position and structure of the visceral organs such as the heart, stomach, spleen, and liver. Mutations that result in a mirror-image reversal of left-right visceral asymmetry have been described in mice (the inver-

sus viscerum or *iv* mutation) (1, 2) and in humans (3, 4), but these mutants reverse left-right polarity only approximately 50% of the time. This suggests that these mutations produce an indeterminate condition of laterality (5) or random determination of polarity (2). Here, we report a recessive insertional mutation that results in situs inversus in 100% of homozygous transgenic mice.

The transgenic family OVE210 was generated by microinjection of the Ty811C tyrosinase minigene into one-cell-stage embryos of the inbred albino mouse strain FVB/N (6). At birth, transgenic mice can be identified by the presence of pigmentation in their eyes; hemizygous adult mice have light brown fur pigmentation. Southern (DNA) hybridizations to tail DNAs revealed that the OVE210 mice have a single site of transgene integration with a low copy number (one to two copies per genome) (7). When hemizygous transgenic OVE210 mice were mated together to generate homozygous mice, no viable adult homozygotes were obtained. Inspection of

newborn mice revealed that some of the mice had stomachs located on the right side instead of the left side of the abdomen (Fig. 1A). These mutant mice exhibited severe jaundice (7), did not increase in size or weight after birth (Fig. 1A), and did not survive beyond 7 days of age. Dissection of the mutant newborns revealed that they had a common pattern of situs inversus; each had its stomach and spleen (Fig. 1B) located on the right side instead of the left side of the abdomen. Orientations of the heart (Fig. 1B), lungs, and liver were also mirror-image left-right inversions.

To determine the percentage of embryos with situs inversus, we mated hemizygote OVE210 mice and terminated the pregnancies between embryonic day 16 (E16) and E19. The fetuses were assayed for ocular pigmentation and visceral orientation. Out of a total of 74 fetuses, 16 (22%) were albino with normal polarity, 41 (55%) were pigmented with normal polarity, and 17 (23%) were pigmented and had situs inversus, which suggests that insertion of the transgene had caused a recessive mutation. Fifteen of the situs inversus mice were examined in detail. All 15 had left-right reversal of their abdominal visceral organs, one had polysplenia, and one had normal cardiovascular orientation (levocardia) even though the abdominal viscera were inverted (a condition termed heterotaxia). Histological examination of the visceral organs revealed that the mutant mice had significant kidney pathology with dilated tubules and abnormal glomeruli (7). When assayed by Southern hybridization, the fetus with heterotaxia was found to be homozygous for the transgenic insertion.

Kartagener's syndrome (3) is an autosomal recessive disorder in humans characterized by situs inversus. The syndrome is associated with chronic sinusitis and pulmonary disease, in addition to infertility in males. Patients with Kartagener's syndrome exhibit defective dynein arms in their cilia (8). To assess whether the transgenic mice with situs inversus might have a similar defect, we collected tracheae from mutant and control mice and examined the tracheal cilia by electron microscopy. No defects in the dynein arms were observed in the transgenic mutants (9).

To begin molecular characterization of this new insertional mutation, we constructed a genomic library of OVE210 DNA (10–13). Four overlapping clones containing the transgenic integration site were obtained (Fig. 2A). One clone (clone 4) contains the entire transgenic insert (two tandem copies of the transgene). A 2.0-kb Hind III fragment (p3.2H) (Fig. 2A) that contained single-copy genomic sequences was used as a probe in Southern hybridizations to verify that the mutant mice were

T. Yokoyama, Department of Cell Biology, Baylor College of Medicine, Houston, TX 77030.

N. G. Copeland and N. A. Jenkins, Mammalian Genetics Laboratory, ABL-Basic Research Program, National Cancer Institute, Frederick Cancer Research and Development Center, Frederick, MD 21702.

C. A. Montgomery, Center for Comparative Medicine, Baylor College of Medicine, Houston, TX 77030.

F. F. B. Elder, Department of Pathology and Laboratory Medicine, University of Texas Health Science Center, Houston, TX 77030.

P. A. Overbeek, Department of Cell Biology, Institute for Molecular Genetics, and Howard Hughes Medical Institute, Baylor College of Medicine, Houston, TX 77030.

*To whom correspondence should be addressed.